NANO LETTERS

pubs.acs.org/NanoLett Letter

Evidence for Topological Magnon–Phonon Hybridization in a 2D Antiferromagnet down to the Monolayer Limit

Jiaming Luo, Shuyi Li, Zhipeng Ye, Rui Xu, Han Yan, Junjie Zhang, Gaihua Ye, Lebing Chen, Ding Hu, Xiaokun Teng, William A. Smith, Boris I. Yakobson, Pengcheng Dai, Andriy H. Nevidomskyy,* Rui He,* and Hanyu Zhu*

Cite This: *Nano Lett.* 2023, 23, 2023–2030 Read Online

ACCESS | Metrics & More | Article Recommendations | Supporting Information

ABSTRACT: Topological phonons and magnons potentially enable low-loss, quantum coherent, and chiral transport of information and energy at the atomic scale. Van der Waals magnetic materials are promising to realize such states due to their recently discovered strong interactions among the electronic, spin, and lattice degrees of freedom. Here, we report the first observation of coherent hybridization of magnons and phonons in monolayer antiferromagnet $FePSe_3$ by cavity-enhanced magneto-Raman spectroscopy. The robust magnon–phonon cooperativity in the 2D limit occurs even in zero magnetic field, which enables nontrivial band inversion between longitudinal and transverse optical phonons caused by the strong coupling with magnons. The spin and lattice symmetry theoretically guarantee magnetic-field-controlled topological phase transition, verified by nonzero Chern numbers calculated from the coupled spin–lattice model. The 2D topological magnon–phonon hybridization potentially offers a new route toward quantum phononics and magnonics with an ultrasmall footprint.

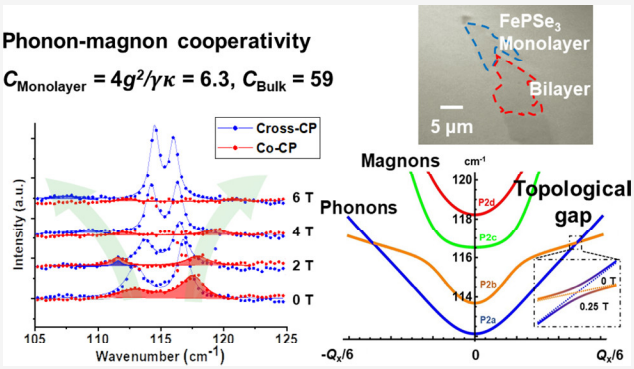

KEYWORDS: *two-dimensional antiferromagnets, magnon–phonon hybridization, chiral topological phonons, terahertz magnons in monolayers*

Nondegenerate bosonic topological bands with nonzero Chern number[1−4] can lead to quantum Hall-like topological channels that are completely independent of material's geometry and immune to any elastic scattering, as opposed to quantum spin Hall materials or topological semimetals.[5] Such chiral topological bosons require time-reversal symmetry breaking, usually provided by magnetic materials or magnetic fields, and were first experimentally demonstrated in a coupled mode of microwave photons and tunable ferromagnetic resonance (magnons).[6] Phononics and magnonics without photons are advantageous for more compact topological devices because their wavelengths can be as small as atomic unit cells.[7,8] Bulk magnonic topological insulators with helical edge states have been experimentally demonstrated in kagomé and honeycomb lattice ferromagnets[9−12] and theoretically expected for single molecular layers,[13,14] but whether nontrivial chiral states exist or survive in real nanomaterials is an open question. Similarly, tunable topological phononic gaps have been theoretically proposed in numerous two-dimensional models with spin–phonon coupling,[15−20] but there are yet no materials suitable to test these predictions. The major challenge is that in typical magnetic materials the coherent coupling between magnon and phonon bands (denoted by g) is weak compared to the dissipation rates of the respective bosons (denoted by γ and κ, respectively), i.e., the quantum cooperativity $C = 4g^2/\gamma\kappa \lesssim 1$. Consequently, the phonons and magnons can incoherently convert into each other but do not form isolated topologically nontrivial bands.[21−23] Very recently, van der Waals (vdW) magnetic materials,[24−31] particularly antiferromagnets (AFMs) such as $FePS_3$, were discovered to exhibit much higher magnon–phonon cooperativity than conventional materials and may overcome this challenge.[32−35] However, it is unclear if the cooperativity can survive in the monolayer limit or if the hybridized magnon–phonon bands exhibit topological properties.

Here we report magnon–phonon hybridization in a vdW antiferromagnet $FePSe_3$ in the monolayer limit with evidence

Received: January 29, 2023
Revised: February 14, 2023
Published: February 16, 2023

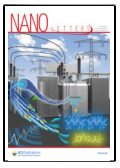

https://doi.org/10.1021/acs.nanolett.3c00351
Nano Lett. 2023, 23, 2023–2030

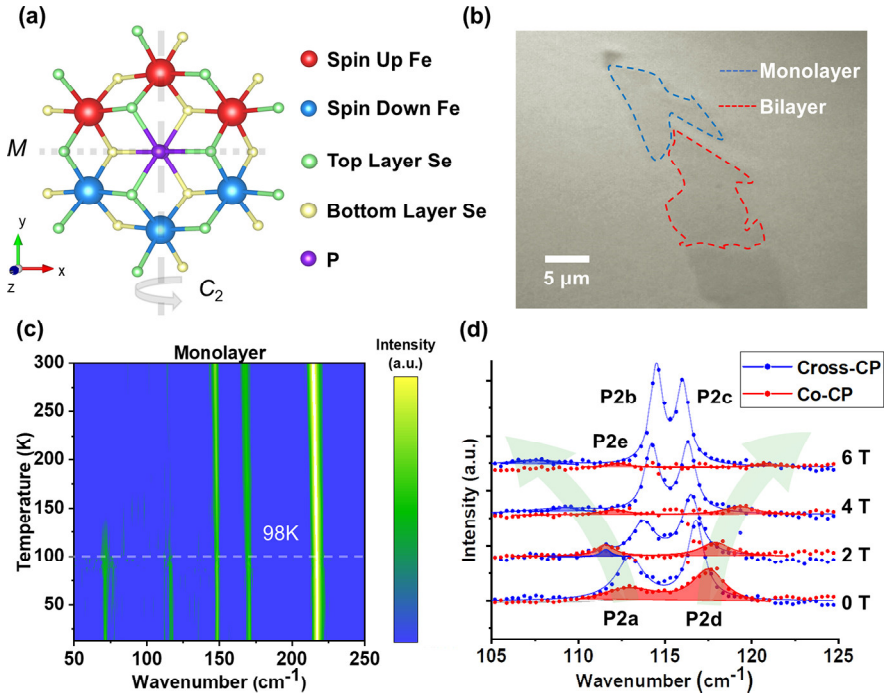

Figure 1. Magnon–phonon hybridization in a two-dimensional antiferromagnet. (a) Crystalline and magnetic structures of $FePSe_3$ in a single conventional unit cell. The hexagonal Fe^{2+} lattice is slightly distorted in zigzag magnetic order but retains the 2-fold rotational, mirror, and $t_{1/2}T$ symmetry. (b) Optical image of the investigated monolayer and bilayer samples inside the Raman-enhanced cavity. (c) Temperature-dependent Raman spectrum of the monolayer shows abruptly enhanced Raman activities near 70 and 115 cm^{-1}, indicating the antiferromagnetic phase transition with a Néel temperature of 98 K. (d) Circular-polarization-resolved magneto-Raman spectrum of the monolayer at 12 K. A pair of field-dependent magnon modes hybridize with a pair of phonon modes under zero magnetic field and then separate and decouple under high fields.

of nontrivial topology. We discovered that the optically active magnons and phonons strongly couple with large cooperativity of $C = 6.3 \pm 1.0$, which may potentially be improved to the bulk value of 59 ± 7, using polarization-resolved magnetic-field-dependent Raman spectroscopy. The accidental degeneracy of optical phonons and magnons is facilitated by the unusually high frequencies of magnonic lower branches due to large magnetic anisotropy of the high-spin ($S = 2$) Fe^{2+} ions.[36] The finite coupling between in-plane phonons and magnons at the zone center indicates anisotropic spin-exchange interactions that have not been considered in previous studies of vdW antiferromagnets.[33,35] We observed band inversion between the longitudinal and transverse optical magnon–phonon hybrid bands due to the anisotropic zigzag magnetic structure of $FePSe_3$ (Figure 1a). The magnetic group symmetry also protects the topological crossing between bands in zero field, which theoretically allows a topologically nontrivial band gap to open under external magnetic fields.[37,38] The stable 2D magnetism protected by large single-ion anisotropy results in robust magnon–phonon cooperativity for possible topological magnon–phonon bands at temperatures as high as 50 K. Our discovery provides the first material example of 2D topological magnon–phonon modes and establishes $FePSe_3$ as a promising platform for experimentally studying topological phononic and magnonic transport. In addition, the magnon–phonon cooperativity could potentially enable quantum coherent phononic and spintronic nanodevices.[39,40]

First, we experimentally observed coupled magnons and phonons in monolayer and bilayer $FePSe_3$ crystals through cavity-enhanced magneto-Raman spectroscopy. Stable magnons have been found in ferromagnetic monolayers including Fe and CrI_3 through electron energy loss spectroscopy and Raman spectroscopy,[41,42] but magnons in similar AFM have much smaller scattering cross section and have not been clearly detected in thicknesses below four layers.[33,35] Therefore, we employ a cavity which enhances the Raman cross section by about 15 times (Experimental Methods and Figure S1) and protects the ultrathin crystals (Figures 1b and S2) from degradation. $FePSe_3$ belongs to a family of 2D transition phosphorus trichalcogenides MPX_3 (where M = Mn, Fe, Ni, etc., and X = S, Se) with stable magnetic order in the monolayer limit[43–45] and unique light–matter interactions, such as magnetic-order-dependent photoluminescence, linear dichroism, and second-harmonic generation.[26–31] Despite the same honeycomb structure, the difference in exchange interactions leads to distinctive magnetic orders and group symmetry among the MPX_3 materials.[46] We discovered a symmetry-breaking phase transition near $T_N = 98$ K in monolayer $FePSe_3$ (compared with 110 K in the bulk), with two prominently enhanced features around 75 cm^{-1} (P1) and 115 cm^{-1} (P2) (Figure 1c). The phase transition and the spectral features resemble those of bulk $FePSe_3$, which develops a zigzag AFM order along the X-axis with spins aligning along the Z-axis according to inelastic neutron scattering.[47,48] Thus, we assign the same AFM order to monolayer $FePSe_3$ indirectly, as the inelastic neutron scattering is not feasible for monolayers. Both aforementioned features P1 and P2 are E_g modes in the cross-circular-polarization (cross-CP) scattering channel above T_N.[49] Below T_N, the magnetic order and the associated lattice distortion lower the point group symmetry from D_{3d} to C_{2h} but preserve the 2-fold symmetry C_2 along the Y-axis, the mirror symmetry M_y with respect to the XZ plane, and the symmetry $t_{1/2}T$, where T is

https://doi.org/10.1021/acs.nanolett.3c00351
Nano Lett. 2023, 23, 2023–2030

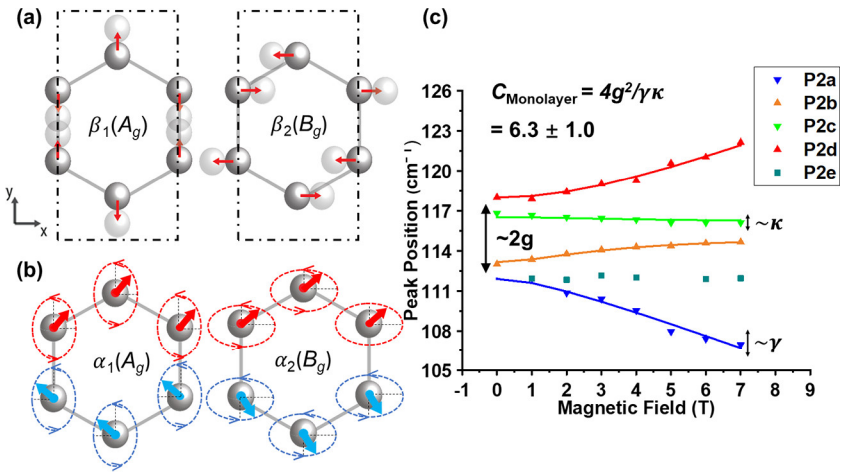

Figure 2. Microscopic modeling of the magnon−phonon hybridization. (a) Displacement of Fe^{2+} ions according to first-principles calculations for the two phonon eigenmodes near the observed P2 frequency. (b) Calculated spin precession from the exchange coupling model includes both the isotropic Heisenberg interactions and the anisotropic Kitaev interactions. (c) Theoretical field-dependent frequencies of the hybrid modes agree with the observed peaks in the magneto-Raman spectrum at 12 K. The extracted magnon−phonon cooperativity in the monolayer is 6.3 ± 1.0. The uncertainty is calculated from the standard deviations of the fitting parameters.

the time-reversal operation and $t_{1/2}$ is a half-magnetic-unit-cell translation operation.[4] Thus, each E_g doublet is expected to split into one antisymmetric B_g mode, whose Raman signal stays in the cross-CP channel, and one symmetric A_g mode, whose Raman signal has a small leak into the co-circular-polarized (co-CP) channel (Supporting Information Section 8). We did not use linearly polarized bases to determine the mode symmetry because the sample contains a mixture of domain orientations.[31,50] While P1 indeed follows this expectation, P2 instead evolves into multiple distinguishable peaks of strongly coupled phonons and magnons, which have never been resolved in previous studies of bulk $FePSe_3$ (Figure 1d).[51,52]

We then determined the composition and symmetry of the hybrid magnon−phonon modes by the magnetic field dependence Raman spectrum at 12 K. Under an applied field B along the Z-axis from 0 to 7 T, P1 changes in neither intensity nor frequency, as expected for pure phonon modes (Figure S3). In contrast, 4 out of 5 features of P2 are notably field-dependent and must have magnon components. P2a and P2d (Figure 1d) shift away from the center of P2 and asymptotically approach a linear dependence on the magnetic field strength ($\hbar\Delta\omega/B$ = 0.98 ± 0.05 cm^{-1}/T corresponding to a g factor of 2.1 ± 0.05, fitted from our theoretical model in the Supporting Information Section 9E), which is a signature of antiferromagnetic magnons. P2b and P2c exhibit significant shifts that saturate at higher magnetic fields, resulting from phonons hybridized to the magnons. Such coherently strong-coupled magnons and phonons are often called "magnon−polarons" analogous to magnon−polaritons,[53,54] despite the fact that the hybrid mode consists of a single phonon mode with well-defined momentum, unlike polarons which are surrounded by a cloud of localized phonons. To identify the symmetry of these modes, we note that although A_g and B_g symmetry representations are only strictly defined at zero magnetic field, the polarization selection rule should not abruptly change at a finite magnetic field. We found that P2a remains primarily cross-CP, thus indicating approximate B_g symmetry, while P2d remains primarily co-CP, corresponding to nearly A_g symmetry. Lastly, P2e in the co-CP channel does not shift under magnetic field, a behavior expected for uncoupled A_g phonons. No significant field-dependent changes of energy or polarization selection rule were found for other Raman modes, meaning the magneto-phonon resonance and magneto-optic effects are weak in this material.[55−58] We further obtained the atomic displacements and corroborated the symmetries of these phonon modes by comparing the experimental Raman spectrum with density functional theory calculations. For the nonmagnetic phase above T_N, our first-principles calculations reproduced the relative positions of all eight Raman-active phonon modes and their respective symmetries (A_{1g} or E_g). After that, we imposed the zigzag AFM order and found that the calculated Raman shifts agree with the experimental values within 10% (Table S1). The phonon modes that contribute to P2, illustrated in Figure 2a as β_1 (with A_g symmetry) and β_2 (with B_g symmetry), show large Fe^{2+} ionic displacements that are expected to notably impact spin-exchange interactions.[48] Meanwhile, the phonon mode P2e contains mainly out-of-plane displacement of Fe^{2+} ions, which does not change the interionic distances to the first-order approximation.

The symmetric/antisymmetric assignments can be extended to modes along the high-symmetry lines in the Brillouin zone at zero magnetic field. For example, on the Γ−X line, the phonon wavevectors have $q_x \neq 0$ and $q_y = 0$, which break the C_2 symmetry but still obey the M_y symmetry. The wave function of the symmetric P2a peak mainly consists of β_2 component, i.e., the longitudinal optical (LO) phonon with respect to the propagation along the Γ−X direction. The wave function of the antisymmetric P2b peak mainly consists of the β_1 component, the transverse optical (TO) phonon. In typical materials, LO usually has higher energy than the pairing TO throughout the Brillouin zone, but here we observed that P2a has lower energy than P2b due to magnon−phonon hybridization, indicating band inversion at the Γ point. Therefore, we expect a mirror-symmetry-protected band crossing between the symmetric and antisymmetric hybrid modes. A finite magnetic field will open a $(t_{1/2}T)$-breaking gap between the two crossing bands when both bands contain magnon components. Such a gap will lead to nontrivial topological bands, similar to the mechanism that forms chiral edge states in surface-magnetized topological insulators.[59] Thus, the

https://doi.org/10.1021/acs.nanolett.3c00351
Nano Lett. 2023, 23, 2023−2030

observed symmetries from Raman selection rule may guarantee field-tunable nontrivial topology in the hybrid magnon–phonon bands outside the Γ point.

To verify the band topology with microscopic modeling, we calculated the spin–lattice interaction and the coupling constant in monolayer $FePSe_3$ based on the measured magnon–phonon hybridization. Although no neutron scattering data are available for the momentum-resolved magnon band structures of $FePSe_3$ in the literature, we assume the spin-exchange interactions resemble those of $FePS_3$ based on the similarity of their magnetic order, except that the interaction constants scale with T_N.[60] The magnon Hamiltonian H_{spin} includes fixed values of first, second, and third nearest-neighbor (NN) Heisenberg interactions as well as two variable parameters of single-ion anisotropy and bond-dependent anisotropic exchange interaction (Supporting Information Section 9A). The pure magnons at the Γ point contain a pair of low-energy modes $\alpha_{1,2}$, with their respective symmetries shown in Figure 2b at P2 wavenumber and a pair of well-separated, high-energy modes above 300 cm^{-1}. At zero field, the magnon eigenmodes neither break $(t_{1/2}T)$ symmetry nor possess net angular momentum due to the anisotropic zigzag magnetic order. The spin exchange parameters are functions of interatomic distance, giving rise to spin–lattice coupling, which is known to be strong in $FePX_3$, as the magnetic order distorts the lattice by as much as 0.3% (Supporting Information Section 9C).[48] We found that to the first-order approximation, the isotropic Heisenberg interaction or possible Dzyaloshinskii–Moriya interaction does not contribute to the coupling between magnon and in-plane phonons at the Γ point due to the volume conservation and inversion symmetry of the phonon modes, respectively. Thus, the magnon–phonon coupling should originate from the dependence of anisotropic spin exchange interaction on bond length (Supporting Information Section 9C). This mechanism differs from the ones proposed for the out-of-plane phonons in $FePS_3$[33,35] or for the in-plane phonons in Néel-type AFM.[20] Our model accurately reproduced the magnetic-field-dependent hybrid modes (Figure 2c and Supporting Information Section 9E). From the fitted spin–lattice coupling coefficient, we calculated the coupling constant between the antisymmetric phonon β_2 and magnon α_2 to be $\hbar g = 2.6 \pm 0.3$ cm^{-1}, or 0.32 ± 0.04 meV in zero field. Together with the line widths extracted from nearly decoupled phonons and magnons at 7 T, we can estimate the quantum cooperativity in the monolayer $FePSe_3$ to be 6.3 ± 1.0, allowing one magnon to coherently convert to one phonon with the same energy and momentum with high fidelity.[61] We note that in finite magnetic fields, all four modes couple with each other, so a single-valued coupling constant must be replaced by a coupling matrix between magnons and phonons. The elements in the coupling matrix and the effective cooperativity among the modes become functions of the magnetic field but are still within the same order of magnitude. We also emphasize that the choice of other possible microscopic models and/or parameters will not qualitatively affect the calculated cooperativity or the symmetry-enabled nontrivial topology.

Using the microscopic model of spin–lattice interactions, we visualized the topological transition of hybrid magnon–phonon modes in the band diagram along the $\bar{X}$–Γ–X line (Figure 3a). To analytically express the phononic energy and wave functions, we adapted a quadratic approximation within $|q_x| < Q_x/6$ and $|q_y| < Q_y/8$, where the $\beta_{1,2}$ branches are isolated

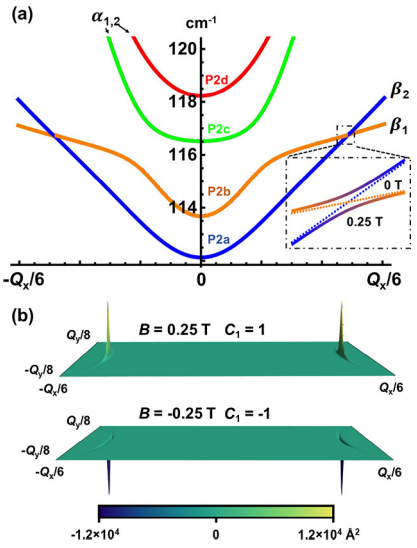

Figure 3. Nontrivial topology of hybrid magnon–phonon bands in monolayer $FePSe_3$. (a) Band structure along the X-axis at B = 0 T shows a protected crossing between the inverted symmetric and antisymmetric bands. Inset: a topological band gap opens under a small magnetic field. (b) Calculated Berry curvature of the lowest band at B = 0.25 T is nonzero and switches sign at B = −0.25 T, confirming a topological transition at B = 0 T.

from other in-plane optical phonon bands (Supporting Information Section 9B). Here Q_x and Q_y are the reciprocal lattice constants along the X- and Y-axis, respectively. The effective masses of the two phonons were obtained by fitting the DFT-calculated phonon dispersion. The numerical solution of the fully coupled spin–lattice Hamiltonian confirmed the presence of band crossing at zero magnetic field. When $|q_x| \gg Q_x/6$, the magnons and phonons decouple because the magnon bands have much larger dispersion. Therefore, the wave function of the symmetric P2a band mainly consists of the β_2 component, which is the longitudinal phonon with respect to the propagation direction, while the wave function of the antisymmetric P2b band mainly consists of the β_1 component, which is the transverse phonon. The longitudinal phonon has a higher energy than the transverse phonon as expected for typical materials. When $|q_x| \to 0$, the P2a band becomes the hybridization of α_1 and β_1 and inverts in energy relative to the P2b band, which is the result of hybridization of α_2 and β_2. The magnon components α_1 and α_2 in the crossing bands can couple under an external out-of-plane magnetic field, so a gap opens up between P2a and P2b (see the inset in Figure 3a). This field-induced gap is different from but directly depends on, the hybridization gap that we observed at the Γ point because without hybridizations the two phonon bands will not interact. We calculated the Berry curvature $\Omega_n(k)$ and the Chern number C_n of all four magnon–phonon hybrid bands considered in our phenomenological model at $B = \pm 0.25$ T. The lowest band has nonzero Berry curvature concentrated at the gap opening regions, which changes sign when we reverse the magnetic field (Figure 3b). The lowest band Chern number is ±1 for positive/negative magnetic field and is insensitive to the model's fitting parameters, proving the robustness of the topological phase transition in an applied field. These calculated Chern numbers from our minimal model do not necessarily hold when we consider other symmetry-protected

https://doi.org/10.1021/acs.nanolett.3c00351
Nano Lett. 2023, 23, 2023–2030

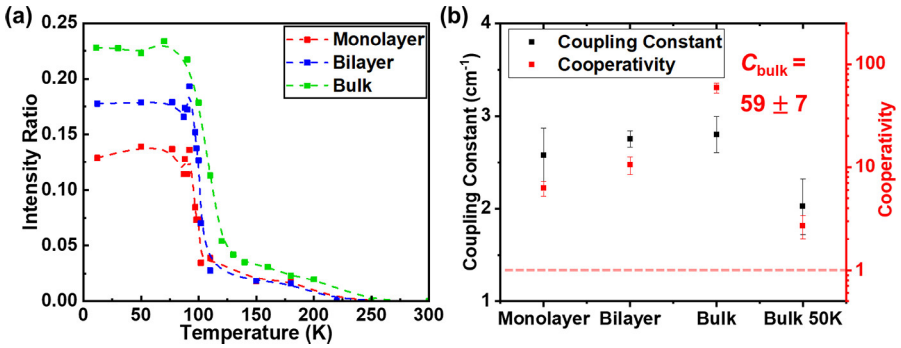

Figure 4. Thickness independence and thermal stability of the magnetic order and magnon−phonon cooperativity in $FePSe_3$. (a) Temperature-dependent Raman acitivity of P2 shows only a minor reduction of 14 K in Néel temperature from bulk to monolayer, indicating weak interlayer coupling. (b) Magnon−phonon coupling constant $\hbar g$ (left axis) is stable with respect to the layer number and temperature, meaning the quantum cooperativity is extrinsically limited by line width. The cooperativity survives at an elevated temperature of 50 K in bulk $FePSe_3$. The error bars are calculated from the 95% confidence interval of the fitting parameters.

phonon−phonon and magnon−phonon band crossings inside the entire Brillouin zone because such crossings can develop additional topological gaps. Yet, including more topologically trivial phonon bands will not affect the existence of the nontrivial topology.

Finally, we found that the robustness of topology and the magnon−phonon cooperativity of monolayers are not yet limited by intrinsic materials properties and can be potentially improved by an order of magnitude in the future. We first confirmed that the magnetism and T_N of $FePSe_3$ are less sensitive to the number of layers compared with other 2D materials (Supporting Information Section 10).[62] The Néel temperatures of multilayers are determined by the sharp transition of temperature-dependent, normalized total Raman activity of the P2 mode (Figures 4a and S6). Remnant lattice distortion-enhanced Raman scattering beyond T_N shows robust short-range spin correlation. Other intrinsic material properties, such as the energy of the hybrid modes and the magnon−phonon coupling constant g, are comparable in monolayer, bilayers, and 10 nm thick bulk crystals at temperatures from 12 K up to 50 K. Promisingly, the magnon−phonon cooperativity rapidly increases from 6.3 ± 1.0 in the monolayer, to 10.5 ± 2.1 in the bilayer, and ultimately to 59 ± 7 in the bulk, the largest value reported so far (Figures 4b and S7).[32] The main reason for higher cooperativity is the smaller line widths of the hybrid modes, i.e., 0.7 cm^{-1} in the bulk compared with 2.1 cm^{-1} the monolayer. The larger line width in monolayers may have multiple extrinsic origins, including more scattering from the substrate, greater strain inhomogeneity induced by the substrate, and more surface defects caused by exposure to the ambient environment. Note that the measured bulk line widths may be larger than their true values due to non-negligible instrument broadening and the scattering by domain boundaries,[31] so the real cooperativity could be higher. Given the stable intrinsic 2D magnetism in monolayers, we expect that the intrinsic homogeneous line widths and cooperativity should be comparable for high-quality, encapsulated monolayers and bulk $FePSe_3$. Narrower line width will enable well-defined chiral edge states if the topological gap is enlarged to exceed the line width by stronger magnetic fields or exchange bias (Figure S5). The topological states will also be robust against minor deviation of the magnetic order in thin layers from the bulk zigzag AFM order. Such symmetry breaking may arise from the change of the interlayer exchange couplings or the substrate effect from bulk to 2D, but these interactions are known to be negligible compared with the scale of the magnon−phonon coupling and the topological gap.[63] To the best of our knowledge, no experimental means can directly measure such band inversion with a magnonic or phononic topological gap with sufficient energy resolution. Inelastic neutron scattering, for example, has an instrumental line width much larger than the topological gap in $FePSe_3$. Meanwhile, the nontrivial topology may manifest itself through indirect measurements, such as thermal Hall effects and nonlinear optical spectroscopy in future studies. The edge transport is not yet immune to bulk scattering because $FePSe_3$ does not possess a full topological gap, but the simple principle of topological phononics illustrated by our work will hopefully help identify new materials with fully protect chiral edge states through high-throughput computation.[40]

In summary, we have experimentally observed topological magnon−phonon hybridization in the monolayer $FePSe_3$. The nontrivial topology is enabled by the zigzag AFM order, the structural mirror symmetry, and field-controlled time-reversal symmetry breaking. A finite magnetic field opens a topological gap, potentially resulting in a large Berry curvature of the hybridized bands or bosonic chiral edge states. Both the topology and the large magnon−phonon cooperativity are intrinsically robust in the 2D limit. The coherent magnon−phonon conversion in ultrathin crystals may enable novel quantum phononic and magnonic devices for hybrid quantum nanosystems,[64] which operate in terahertz frequencies and at higher temperatures than those needed for microwave quantum circuits.[65,66] The external field tunability of magnons potentially allows us to reconfigure bosonic chiral edge states at the atomic scale.[67−69] In addition, the measured sensitivity of bond-dependent (Kitaev-like) anisotropic interactions to atomic displacements may facilitate phononic engineering of exotic magnetic phases.[70]

■ ASSOCIATED CONTENT

Data Availability Statement

The data sets generated during and/or analyzed during this study are available from the corresponding author on reasonable request.

Supporting Information

The Supporting Information is available free of charge at https://pubs.acs.org/doi/10.1021/acs.nanolett.3c00351.

https://doi.org/10.1021/acs.nanolett.3c00351
Nano Lett. 2023, 23, 2023−2030

Experimental methods, including crystal growth and sample fabrication, Raman measurement and cavity enhancement, and first-principles calculations; additional experimental data on the characterization of monolayer and bilayer $FePSe_3$, magnetic-field dependence of P1 in the monolayer, phase transition in bilayer and bulk, and quantum cooperativity in different thicknesses and temperatures; theoretical model of magnon−phonon hybridization and topological gap under high magnetic field; comparison between calculated Raman-active modes and selection rules with experiments, and the comparison of the phase transition temperature in different van der Waals magnetic materials (PDF)

AUTHOR INFORMATION

Corresponding Authors

Hanyu Zhu − *Department of Materials Science and Nano Engineering, Rice University, Houston, Texas 77005, United States*; orcid.org/0000-0003-3376-5352; Email: Hanyu.Zhu@rice.edu

Rui He − *Department of Electrical and Computer Engineering, Texas Tech University, Lubbock, Texas 79409, United States*; orcid.org/0000-0002-2368-7269; Email: Rui.He@ttu.edu

Andriy H. Nevidomskyy − *Department of Physics and Astronomy, Rice University, Houston, Texas 77005, United States*; Email: Andriy.Nevidomskyy@rice.edu

Authors

Jiaming Luo − *Department of Materials Science and Nano Engineering, Rice University, Houston, Texas 77005, United States; Applied Physics Graduate Program, Rice University, Houston, Texas 77005, United States*

Shuyi Li − *Department of Physics and Astronomy, Rice University, Houston, Texas 77005, United States*

Zhipeng Ye − *Department of Electrical and Computer Engineering, Texas Tech University, Lubbock, Texas 79409, United States*

Rui Xu − *Department of Materials Science and Nano Engineering, Rice University, Houston, Texas 77005, United States*

Han Yan − *Department of Physics and Astronomy, Rice University, Houston, Texas 77005, United States*

Junjie Zhang − *Department of Materials Science and Nano Engineering, Rice University, Houston, Texas 77005, United States*; orcid.org/0000-0002-4779-2725

Gaihua Ye − *Department of Electrical and Computer Engineering, Texas Tech University, Lubbock, Texas 79409, United States*

Lebing Chen − *Department of Physics and Astronomy, Rice University, Houston, Texas 77005, United States*

Ding Hu − *Department of Physics and Astronomy, Rice University, Houston, Texas 77005, United States*

Xiaokun Teng − *Department of Physics and Astronomy, Rice University, Houston, Texas 77005, United States*

William A. Smith − *Department of Materials Science and Nano Engineering, Rice University, Houston, Texas 77005, United States*

Boris I. Yakobson − *Department of Materials Science and Nano Engineering, Rice University, Houston, Texas 77005, United States*; orcid.org/0000-0001-8369-3567

Pengcheng Dai − *Department of Physics and Astronomy, Rice University, Houston, Texas 77005, United States*

Complete contact information is available at: https://pubs.acs.org/10.1021/acs.nanolett.3c00351

Author Contributions

J.L. and H.Z. conceived the experiment. Z.Y., G.Y., J.L., and R.H. performed Raman measurements. J.L. and R.X. fabricated the samples. J.L., R.H., and H.Z. analyzed the experimental data. J.Z. and B.Y. conducted first-principles calculations. S.L., H.Y., L.C., J.L., and H.Z. performed the theoretical modeling. X.T., D.H., and P.D. synthesized the crystals. All authors discussed the results and made contributions to the manuscript.

Notes

The authors declare no competing financial interest.

ACKNOWLEDGMENTS

J.L. and H.Z. are supported by the U.S. National Science Foundation (NSF) Grant DMR-2005096. R.X. and H.Z. acknowledge the support of the Robert A. Welch Foundation Grant C-2128. W.S. and H.Z. acknowledge the support by NSF Grant DMR-2019004. Z.Y., G.Y., and R.H. acknowledge the support by NSF CAREER Grant DMR-1760668 and NSF Grant DMR-2104036. H.Y. and A.H.N. were supported by the NSF Grant DMR-1917511. S.L. and A.H.N. acknowledge the support of the Robert A. Welch Foundation Grant C-1818. P.D.'s single crystal growth effort at Rice is supported by US NSF-DMR-2100741 and the Robert A. Welch Foundation under Grant C-1839. J.Z. and B.I.Y. acknowledge Army Research Office Grant W911NF-16-1-0255. J.L. thanks Nan Cheng for helpful discussions.

REFERENCES

(1) Kim, M.; Jacob, Z.; Rho, J. Recent advances in 2D, 3D and higher-order topological photonics. *Light Sci. Appl.* **2020**, *9*, 130.

(2) Liu, Y.; Chen, X.; Xu, Y. Topological Phononics: From Fundamental Models to Real Materials. *Adv. Funct. Mater.* **2020**, *30*, 1904784.

(3) McClarty, P. Topological Magnons: A Review. *ArXiv210601430 Cond-Mat*, 2021.

(4) Šmejkal, L.; Mokrousov, Y.; Yan, B.; MacDonald, A. H. Topological antiferromagnetic spintronics. *Nat. Phys.* **2018**, *14*, 242−251.

(5) Narang, P.; Garcia, C. A. C.; Felser, C. The topology of electronic band structures. *Nat. Mater.* **2021**, *20*, 293−300.

(6) Wang, Z.; Chong, Y.; Joannopoulos, J. D.; Soljačić, M. Observation of unidirectional backscattering-immune topological electromagnetic states. *Nature* **2009**, *461*, 772−775.

(7) Zhang, L.; Ren, J.; Wang, J.-S.; Li, B. Topological Nature of the Phonon Hall Effect. *Phys. Rev. Lett.* **2010**, *105*, 225901.

(8) Takahashi, R.; Nagaosa, N. Berry Curvature in Magnon-Phonon Hybrid Systems. *Phys. Rev. Lett.* **2016**, *117*, 217205.

(9) Zhang, L.; Ren, J.; Wang, J.-S.; Li, B. Topological magnon insulator in insulating ferromagnet. *Phys. Rev. B* **2013**, *87*, 144101.

(10) Chisnell, R.; et al. Topological Magnon Bands in a Kagome Lattice Ferromagnet. *Phys. Rev. Lett.* **2015**, *115*, 147201.

(11) Chen, L.; et al. Topological Spin Excitations in Honeycomb Ferromagnet CrI_3. *Phys. Rev. X* **2018**, *8*, 041028.

(12) Zhu, F.; et al. Topological magnon insulators in two-dimensional van der Waals ferromagnets CrSiTe3 and $CrGeTe_3$: Toward intrinsic gap-tunability. *Sci. Adv.* **2021**, *7*, No. eabi7532.

(13) Owerre, S. A. A first theoretical realization of honeycomb topological magnon insulator. *J. Phys.: Condens. Matter* **2016**, *28*, 386001.

(14) Aguilera, E.; Jaeschke-Ubiergo, R.; Vidal-Silva, N.; Torres, L. E. F. F.; Nunez, A. S. Topological magnonics in the two-dimensional van der Waals magnet CrI3. *Phys. Rev. B* **2020**, *102*, 024409.
(15) Thingstad, E.; Kamra, A.; Brataas, A.; Sudbø, A. Chiral Phonon Transport Induced by Topological Magnons. *Phys. Rev. Lett.* **2019**, *122*, 107201.
(16) Zhang, X.; Zhang, Y.; Okamoto, S.; Xiao, D. Thermal Hall Effect Induced by Magnon-Phonon Interactions. *Phys. Rev. Lett.* **2019**, *123*, 167202.
(17) Zhang, S.; Go, G.; Lee, K.-J.; Kim, S. K. SU(3) Topology of Magnon-Phonon Hybridization in 2D Antiferromagnets. *Phys. Rev. Lett.* **2020**, *124*, 147204.
(18) Shen, P.; Kim, S. K. Magnetic field control of topological magnon-polaron bands in two-dimensional ferromagnets. *Phys. Rev. B* **2020**, *101*, 125111.
(19) Huang, H.; Tian, Z. Topological phonon-magnon hybrid excitations in a two-dimensional honeycomb ferromagnet. *Phys. Rev. B* **2021**, *104*, 064305.
(20) Ma, B.; Fiete, G. A. Antiferromagnetic insulators with tunable magnon-polaron Chern numbers induced by in-plane optical phonons. *Phys. Rev. B* **2022**, *105*, L100402.
(21) Man, H.; et al. Direct observation of magnon-phonon coupling in yttrium iron garnet. *Phys. Rev. B* **2017**, *96*, 100406.
(22) Holanda, J.; Maior, D. S.; Azevedo, A.; Rezende, S. M. Detecting the phonon spin in magnon-phonon conversion experiments. *Nat. Phys.* **2018**, *14*, 500−506.
(23) Streib, S.; Vidal-Silva, N.; Shen, K.; Bauer, G. E. W. Magnon-phonon interactions in magnetic insulators. *Phys. Rev. B* **2019**, *99*, 184442.
(24) Gong, C.; et al. Discovery of intrinsic ferromagnetism in two-dimensional van der Waals crystals. *Nature* **2017**, *546*, 265−269.
(25) Jiang, S.; Xie, H.; Shan, J.; Mak, K. F. Exchange magnetostriction in two-dimensional antiferromagnets. *Nat. Mater.* **2020**, *19*, 1295−1299.
(26) Kang, S.; et al. Coherent many-body exciton in van der Waals antiferromagnet $NiPS_3$. *Nature* **2020**, *583*, 785−789.
(27) Shan, J.-Y.; et al. Giant modulation of optical nonlinearity by Floquet engineering. *Nature* **2021**, *600*, 235−239.
(28) Ni, Z.; et al. Imaging the Néel vector switching in the monolayer antiferromagnet $MnPSe_3$ with strain-controlled Ising order. *Nat. Nanotechnol.* **2021**, *16*, 782−787.
(29) Wang, X.; et al. Spin-induced linear polarization of photoluminescence in antiferromagnetic van der Waals crystals. *Nat. Mater.* **2021**, *20*, 964−970.
(30) Ni, Z.; Huang, N.; Haglund, A. V.; Mandrus, D. G.; Wu, L. Observation of Giant Surface Second-Harmonic Generation Coupled to Nematic Orders in the van der Waals Antiferromagnet FePS3. *Nano Lett.* **2022**, *22*, 3283−3288.
(31) Zhang, H.; et al. Cavity-enhanced linear dichroism in a van der Waals antiferromagnet. *Nat. Photonics* **2022**, *16*, 311−317.
(32) Zhang, Q.; et al. Coherent strong-coupling of terahertz magnons and phonons in a Van der Waals antiferromagnetic insulator. *ArXiv210811619 Cond-Mat*, 2021.
(33) Liu, S.; et al. Direct Observation of Magnon-Phonon Strong Coupling in Two-Dimensional Antiferromagnet at High Magnetic Fields. *Phys. Rev. Lett.* **2021**, *127*, 097401.
(34) Vaclavkova, D.; et al. Magnon polarons in the van der Waals antiferromagnet $FePS_3$. *Phys. Rev. B* **2021**, *104*, 134437.
(35) Sun, Y.-J.; et al. Magneto-Raman Study of Magnon-Phonon Coupling in Two-Dimensional Ising Antiferromagnetic FePS3. *J. Phys. Chem. Lett.* **2022**, *13*, 1533−1539.
(36) Lançon, D.; et al. Magnetic structure and magnon dynamics of the quasi-two-dimensional antiferromagnet $FePS_3$. *Phys. Rev. B* **2016**, *94*, 214407.
(37) Jauregui, L. A.; Pettes, M. T.; Rokhinson, L. P.; Shi, L.; Chen, Y. P. Magnetic field-induced helical mode and topological transitions in a topological insulator nanoribbon. *Nat. Nanotechnol.* **2016**, *11*, 345−351.
(38) Lu, Y.-S.; Li, J.-L.; Wu, C.-T. Topological Phase Transitions of Dirac Magnons in Honeycomb Ferromagnets. *Phys. Rev. Lett.* **2021**, *127*, 217202.
(39) Li, N.; et al. Colloquium: Phononics: Manipulating heat flow with electronic analogs and beyond. *Rev. Mod. Phys.* **2012**, *84*, 1045−1066.
(40) Li, J.; et al. Computation and data driven discovery of topological phononic materials. *Nat. Commun.* **2021**, *12*, 1204.
(41) Prokop, J.; et al. Magnons in a Ferromagnetic Monolayer. *Phys. Rev. Lett.* **2009**, *102*, 177206.
(42) Cenker, J.; et al. Direct observation of two-dimensional magnons in atomically thin CrI_3. *Nat. Phys.* **2021**, *17*, 20−25.
(43) Du, K.; et al. Weak Van der Waals Stacking, Wide-Range Band Gap, and Raman Study on Ultrathin Layers of Metal Phosphorus Trichalcogenides. *ACS Nano* **2016**, *10*, 1738−1743.
(44) Lee, J.-U.; et al. Ising-Type Magnetic Ordering in Atomically Thin $FePS_3$. *Nano Lett.* **2016**, *16*, 7433−7438.
(45) Wang, X.; et al. Raman spectroscopy of atomically thin two-dimensional magnetic iron phosphorus trisulfide ($FePS_3$) crystals. *2D Mater.* **2016**, *3*, 031009.
(46) Le Flem, G.; Brec, R.; Ouvard, G.; Louisy, A.; Segransan, P. Magnetic interactions in the layer compounds MPX_3 (M = Mn, Fe, Ni; X = S, Se). *J. Phys. Chem. Solids* **1982**, *43*, 455−461.
(47) Scagliotti, M.; Jouanne, M.; Balkanski, M.; Ouvrard, G.; Benedek, G. Raman scattering in antiferromagnetic $FePS_3$ and $FePSe_3$ crystals. *Phys. Rev. B* **1987**, *35*, 7097−7104.
(48) Jernberg, P.; Bjarman, S.; Wäppling, R. $FePS_3$: A first-order phase transition in a "2D" Ising antiferromagnet. *J. Magn. Magn. Mater.* **1984**, *46*, 178−190.
(49) Hashemi, A.; Komsa, H.-P.; Puska, M.; Krasheninnikov, A. V. Vibrational Properties of Metal Phosphorus Trichalcogenides from First-Principles Calculations. *J. Phys. Chem. C* **2017**, *121*, 27207−27217.
(50) Mao, N.; et al. Direct Observation of Symmetry-Dependent Electron-Phonon Coupling in Black Phosphorus. *J. Am. Chem. Soc.* **2019**, *141*, 18994−19001.
(51) Balkanski, M.; Jouanne, M.; Ouvrard, G.; Scagliotti, M. Effects due to spin ordering in layered MPX_3 compounds revealed by inelastic light scattering. *J. Phys. C Solid State Phys.* **1987**, *20*, 4397−4413.
(52) Wang, X. *Optical Study of Two-Dimensional Ternary and Quaternary Metal Phosphorus Chalcogenide Crystals*; Nanyang Technological University: 2018.
(53) Kikkawa, T.; et al. Magnon Polarons in the Spin Seebeck Effect. *Phys. Rev. Lett.* **2016**, *117*, 207203.
(54) Ausloos, M.; Hubert, L.; Dorbolo, S.; Gilabert, A.; Cloots, R. Magnon-polaron and spin-polaron signatures in the specific heat and electrical resistivity of $La_{0.6}Y_{0.1}Ca_{0.3}MnO_3$ in zero magnetic field and the effect of Mn-O-Mn bond environment. *Phys. Rev. B* **2002**, *66*, 174436.
(55) Kim, Y.; et al. Measurement of Filling-Factor-Dependent Magnetophonon Resonances in Graphene Using Raman Spectroscopy. *Phys. Rev. Lett.* **2013**, *110*, 227402.
(56) Cheng, B.; et al. A Large Effective Phonon Magnetic Moment in a Dirac Semimetal. *Nano Lett.* **2020**, *20*, 5991.
(57) Ji, J.; et al. Giant magneto-optical Raman effect in a layered transition metal compound. *Proc. Natl. Acad. Sci. U. S. A.* **2016**, *113*, 2349−2353.
(58) Huang, B.; et al. Tuning inelastic light scattering via symmetry control in the two-dimensional magnet CrI3. *Nat. Nanotechnol.* **2020**, *15*, 212−216.
(59) Zhang, F.; Kane, C. L.; Mele, E. J. Surface State Magnetization and Chiral Edge States on Topological Insulators. *Phys. Rev. Lett.* **2013**, *110*, 046404.
(60) Ashcroft, N. W.; Mermin, N. D. *Solid State Physics*; Holt, Rinehart and Winston: 1976.
(61) Kittel, C. Interaction of Spin Waves and Ultrasonic Waves in Ferromagnetic Crystals. *Phys. Rev.* **1958**, *110*, 836−841.

https://doi.org/10.1021/acs.nanolett.3c00351
Nano Lett. 2023, 23, 2023−2030

(62) Chen, L.; et al. Magnetic anisotropy in ferromagnetic CrI3. *Phys. Rev. B* **2020**, *101*, 134418.
(63) Wiedenmann, A.; Rossat-Mignod, J.; Louisy, A.; Brec, R.; Rouxel, J. Neutron diffraction study of the layered compounds $MnPSe_3$ and $FePSe_3$. *Solid State Commun.* **1981**, *40*, 1067−1072.
(64) Lachance-Quirion, D.; Tabuchi, Y.; Gloppe, A.; Usami, K.; Nakamura, Y. Hybrid quantum systems based on magnonics. *Appl. Phys. Express* **2019**, *12*, 070101.
(65) Zhitomirsky, M. E.; Chernyshev, A. L. Colloquium: Spontaneous magnon decays. *Rev. Mod. Phys.* **2013**, *85*, 219−242.
(66) Caldwell, J. D.; et al. Low-loss, infrared and terahertz nanophotonics using surface phonon polaritons. *Nanophotonics* **2015**, *4*, 44−68.
(67) Mahmoud, A.; et al. Introduction to spin wave computing. *J. Appl. Phys.* **2020**, *128*, 161101.
(68) Dieny, B.; Chshiev, M. Perpendicular magnetic anisotropy at transition metal/oxide interfaces and applications. *Rev. Mod. Phys.* **2017**, *89*, 025008.
(69) Sadovnikov, A. V.; et al. Magnon Straintronics: Reconfigurable Spin-Wave Routing in Strain-Controlled Bilateral Magnetic Stripes. *Phys. Rev. Lett.* **2018**, *120*, 257203.
(70) Disa, A. S.; Nova, T. F.; Cavalleri, A. Engineering crystal structures with light. *Nat. Phys.* **2021**, *17*, 1087−1092.

https://doi.org/10.1021/acs.nanolett.3c00351
Nano Lett. 2023, 23, 2023−2030